Topological properties of subsystem-symmetry-protected edge states in an extended quasi-one-dimensional dimerized lattice

Milad Jangjan and Mir Vahid Hosseini [*]

Department of Physics, Faculty of Science, University of Zanjan, Zanjan 45371-38791, Iran

We theoretically investigate the topological properties of a dimerized quasi-one-dimensional (1D) lattice comprised of multilegs (L) as well as multisublattices (R). The system has main and subsidiary exchange symmetries. In the basis of the latter one, the system can be divided into L 1D subsystems, each of which corresponds to a generalized SSH_R model having R sublattices and on-site potentials. Chiral symmetry is absent in all subsystems except when the axis of the main exchange symmetry coincides on the central chain. We find that the system may host zero- and finite-energy topological edge states. The existence of a zero-energy edge state requires a certain relation between the number of legs and sublattices. As such, different topological phases, protected by subsystem symmetry, including zero-energy edge states in the main gap, no zero-energy edge states, and zero-energy edge states in the bulk states are characterized. Despite the classification symmetry of the system belongs to BDI symmetry class, but each subsystem falls into either AI or BDI symmetry class.

I. INTRODUCTION

Topological states have been engaged in many areas of physics, especially in several systems involving electrons [1–4], cold atoms [5,6], and photons [7] in the past decade [8]. One of the properties of these states is their robustness against disorders or defects [9] as long as the fundamental symmetry of system protecting nontrivial topology is preserved. Symmetries of a system can be used to classify the topology of electronic band structures. Based on topological classification [10–16], a diversity of interesting materials can be categorized into topological insulating [1,17–20], topological superconducting [2,3,21–24], topological semimetal [25–28], and topological metal [29–35] states in one, two, or three dimensions.

In one-dimensional (1D) systems, one of the simplest models for topological insulators is the Su-Schrieffer-Heeger (SSH) chain [36]. It is characterized by two different tunneling amplitudes, i.e., intra- and interunit cell tunneling amplitudes, between two different sublattices in a chain [37]. The SSH chain can host localized edge states at its ends under open boundary conditions in the topologically nontrivial regime. Such a topological state is protected by inversion symmetry and has its topological invariant that can be calculated via bulk states of the band structure under periodic boundary conditions [38]. The generalization of the SSH model, including next-nearest hopping [39], spin-orbit interaction [40,41], and the Zeeman field [41], has also been studied recently. Furthermore, the extended SSH chain, with more than two sublattices per unit cell, comprising three [42] and four [43,44] sublattices, or even [45] and odd [34] numbers of sublattices per unit cell has been investigated in 1D geometry, revealing various topological phases protected by main symmetries of the whole system.

On the other hand, there are interesting 2D systems hosting topological phases [46,47]. A Chern insulator has been proposed in a 2D lattice exhibiting a nonzero quantized Hall conductance in the absence of an external magnetic field [21,22]. Furthermore, helical edge states, protected by time-reversal symmetry, have been realized at the edge of 2D HgTe quantum wells [3]. Interestingly, it has been shown that nontrivial topological phases can be hosted in a 2D SSH model in the absence of Berry curvature due to presence of both time-reversal and inversion symmetries [48].

However, in going from one dimension to two dimensions, one deals with a class of systems, namely, quasi-1D systems, having spectacular features [49]. Simple examples of quasi-1D systems are coupled chains and ladders. Recently, several topological features of ladder lattice structures have been investigated, exhibiting a rich variety of phases based on their topological properties, for instance, topological superconductivity in Kitaev ladder [50]. Also, the effects of spin-orbit coupling [51], interactions [52], and interchain coupling [53] on the topological features of a Creutz ladder as well as the role of topology on the charge-pumping phenomenon in the Creutz ladder [54] have been studied. Beyond the single SSH chain, in a two-leg SSH chain, topological nodal points [55] and non-Abelian Berry connections associated with the glide reflection symmetry [56] have been investigated. Also, chiral solitons [57] and topological bound states [58] have been observed in a coupled double SSH chain. It has also been shown that a dimerized two-leg ladder can host localized and delocalized topological finite-energy edge states in continuum for asymmetric and symmetric dimerization patterns, respectively [32]. However, topological characterization of generalized ladder systems involving more than two legs with multisublattices per leg deserves to be explored further based

*Corresponding author: mv.hosseini@znu.ac.ir
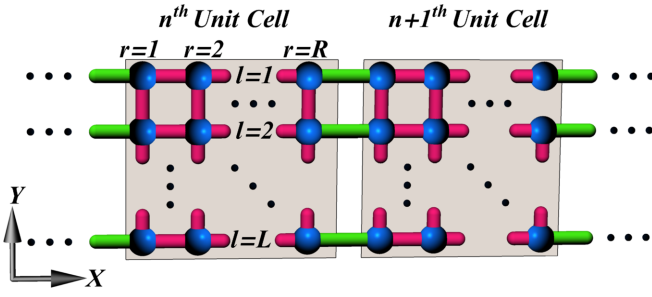
FIG. 1. Schematic geometry of a finite section of quasi-1D lattice comprised of L coupled chains oriented along the x direction. Each chain has R sublattices. Intraunit (interunit) cell hopping, t (t'), represented in red (green) color.

on quasi-1D materials Bi_4X_4 ($X =$ Br, I) [59,60]. Also, it is interesting to find a situation where topological phases are not protected by the main symmetries of the whole system.

In this paper, we consider a quasi-1D dimerized lattice consisting of L legs such that each leg has R sublattices. We will investigate topological properties of the system according to its symmetries. The simultaneous existence of reflection and (main and subsidiary) inversion symmetries allows us to define the so-called main and subsidiary exchange symmetries. The Hamiltonian of the system can be block diagonalized in the basis of subsidiary exchange symmetry with L blocks. Each block can be regarded as a 1D subsystem that resembles the SSH model with R sublattices, SSH_R, having an effective on-site potential. In the topological regime, there are zero- and finite-energy edge states. The system hosts $m - 1$ zero-energy edge states out of $L(R - 1)$ edge states where m is the greatest common divisor of $(L + 1, R)$. Subsequently, depending on the values of L and R, we realize different topological phases: (i) zero-energy edge states reside in the main gap, (ii) there are no zero-energy edge states, and (iii) zero-energy edge states reside within bulk states. By breaking symmetries of the system, interestingly, we realize that the inversion symmetry of subsystems protects the topology of the system.

II. MODEL AND THEORY

We start by considering a quasi-1D superlattice comprising of L number of chains along the x direction and each chain contains R number of sublattices as shown in Fig. 1. The Hamiltonian of the system being the sum of the Hamiltonian of chains, H_{chain}, and the Hamiltonian of interchain couplings, H_{coupl}, is

$$H = H_{\text{chain}} + H_{\text{coupl}},$$

$$H_{\text{chain}} = \sum_{n=1}^{N} \sum_{l=1}^{L} \sum_{r=1}^{R-1} t_l C_{n,l,r}^{\dagger} C_{n,l,r+1}$$

$$+ \sum_{n=1}^{N-1} \sum_{l=1}^{L} t_l' C_{n,l,R}^{\dagger} C_{n+1,l,1} + \text{H.c.},$$

$$H_{\text{coupl}} = \sum_{n=1}^{N} \sum_{l=1}^{L-1} \sum_{r=1}^{R} t_r C_{n,l,r}^{\dagger} C_{n,l+1,r} + \text{H.c.}, \quad (1)$$

where $C_{n,l,r}^{\dagger}$ ($C_{n,l,r}$) is the creation (annihilation) operator of electron on the rth sublattice of the lth chain at the nth unit cell. We take the intracell (intercell) hopping $t_l = t = 1 + \delta_0 \cos(\theta)$ ($t_l' = t' = 1 - \delta_0 \cos(\theta)$) $\forall l \in [1, L]$ in each leg and inter leg hopping $t_r = t = 1 + \delta_0 \cos(\theta)$ $\forall r \in [1, R]$ with δ_0 and θ being the dimerization amplitude and a cyclically varying parameter to control the strength and sign of dimerization, respectively. Also, the N is the number of unit cells. Without loss of generality, we take $\delta_0 = 0.8$ throughout the paper.

Assuming periodic boundary conditions along the chains and using Fourier transform of annihilation (creation) operator $C_{n,l,r}^{(\dagger)} = 1/\sqrt{(N)} \sum_k e^{(-)ikn} C_{k,l,r}^{(\dagger)}$, we can write Hamiltonian Eq. (1) in reciprocal space as $H = \sum_k \langle \psi_k | h(k) | \psi_k \rangle$, where $|\psi_k\rangle = \sum_{l,r}^{L,R} C_{k,l,r} |l\rangle \otimes |r\rangle$ with $|l\rangle$ and $|r\rangle$ being basis states, respectively, in the chain and sublattice spaces and

$$h(k) = \begin{pmatrix} h_{\text{chain}} & h_{\text{coupl}} & \cdots & 0 \\ h_{\text{coupl}} & h_{\text{chain}} & \ddots & 0 \\ \vdots & \ddots & \ddots & h_{\text{coupl}} \\ 0 & \cdots & h_{\text{coupl}} & h_{\text{chain}} \end{pmatrix}_{L \times L}, \quad (2)$$

with

$$h_{\text{chain}} = \begin{pmatrix} 0 & t & \cdots & t'e^{ik} \\ t & & \ddots & \vdots \\ \vdots & \ddots & & t \\ t'e^{-ik} & \cdots & t & 0 \end{pmatrix}_{R \times R},$$

$$h_{\text{coupl}} = \begin{pmatrix} t & 0 & \cdots & 0 \\ 0 & t & \ddots & \vdots \\ \vdots & \ddots & t & 0 \\ 0 & \cdots & 0 & t \end{pmatrix}_{R \times R}.$$

Diagonalizing the bulk Hamiltonian Eq. (2), the spectrum can be obtained having LR bands as shown in Fig. 2 for different values of L and R with $\theta/\pi = 1/2$. One can see that there are some band touching points, indicated by colored dots, at the symmetric points $k = 0$ and $k = \pi$ for $\theta/\pi = 1/2$ (and for $\theta/\pi = 3/2$ not shown). Interestingly, the gap closings at the symmetric points, which may be a signal of topological phase transitions occurring, take place between certain bands at zero (red dots) and/or finite (green dots) energies, depending on the values of L and R. This indicates that there would possibly be zero- and/or finite-energy edge states under open boundary conditions. As shown in Fig. 2(a), the topological band touchings, indicated by red dots, can occur between different bands at zero energy, while the bulk states (blue lines), except at the touching points, do not cross the Fermi level, $E = 0$. This predicts that the zero-energy edge states will reside in the main gap. In contrast, as shown in Fig. 2(b), the topological band touchings, represented by green dots, only exist at finite energies and the bulk states of different bands can be accessed at zero energy. Consequently, in this case, there will be no zero-energy edge states. From Fig. 2(c), one can see, in addition to topological band touching points at zero energy (red dots), bulk states of the other bands are available with the same energy. So, one may anticipate that the zero-energy edge states and the bulk states will coexist. Therefore, these features imply that, correspondingly, there would possibly be
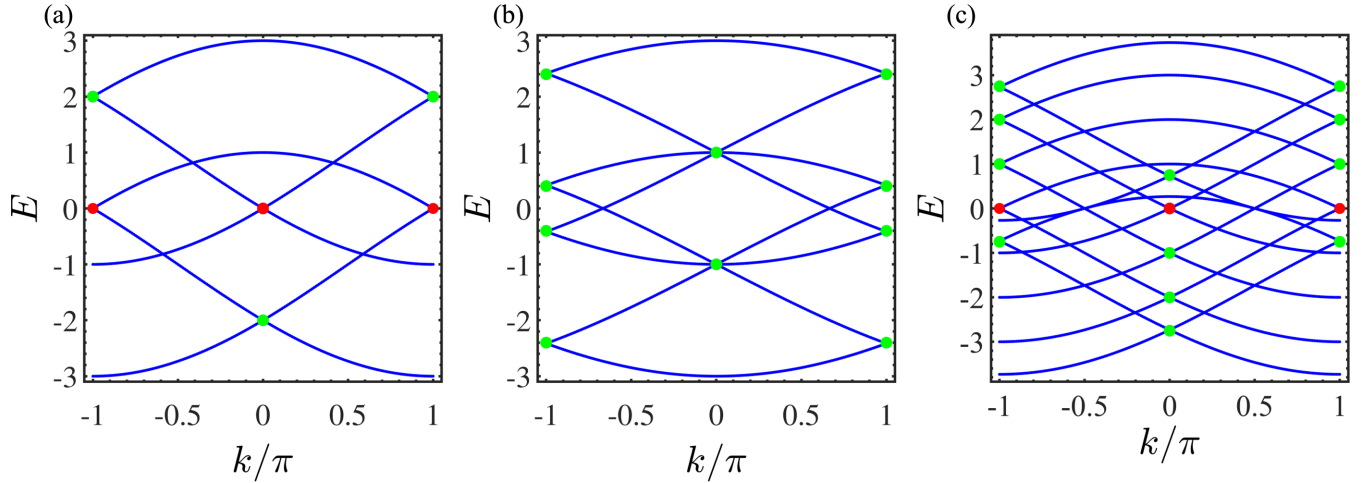
FIG. 2. Energy spectra under periodic boundary conditions for (a) $(L, R) = (2, 3)$, (b) $(L, R) = (2, 4)$, and (c) $(L, R) = (5, 3)$. Here $\theta/\pi = 1/2$. Topological band touching points are shown at zero and finite energies by red and green dots, respectively.

symmetry-protected topological phases associated with zero-energy edge states in the gap, without zero-energy edge states, and with zero-energy edge states in the bulk states. So, we are interested in inspecting symmetries of the system in the following.

III. SYMMETRIES OF THE SYSTEM

A. Main symmetries

In the following, we investigate main symmetries of the system including time-reversal, particle-hole, chiral, and inversion symmetries. The system exhibits time-reversal symmetry defined as $\mathcal{T}_i h(k) \mathcal{T}_i = h(-k)$ with $i = 1, 2$. The operators of time-reversal symmetry are $\mathcal{T}_1 = \tau_{x_L} \otimes I_R \mathcal{K}$ and $\mathcal{T}_2 = I_{LR} \mathcal{K}$, with $\mathcal{K}$ being the complex conjugation, I_L (I_{LR}) is an identity matrix of size L (LR) and

$$\tau_{x_L} = \begin{pmatrix} & & & & 1 \\ & O & & 1 & \\ & & .\cdot^{\cdot} & & \\ & 1 & & O & \\ 1 & & & & \end{pmatrix}_{L \times L}. \tag{3}$$

Note that in this system, $\mathcal{T}_1 = \Upsilon_1 \mathcal{T}_2$, where Υ_1 is a unitary operator and will be investigated below.

Also, the system shows particle-hole and chiral symmetries. Since the system under consideration is a spinless system, the unitary part of particle-hole operator, $\mathcal{P}$, and the chiral operator, Γ, are identical: $\mathcal{P}_1 = \Gamma_1 = \mathcal{C}_{1_L} \otimes \mathcal{C}_{1_R}$ and $\mathcal{P}_2 = \Gamma_2 = \mathcal{C}_{2_L} \otimes \mathcal{C}_{1_R}$, where

$$\mathcal{C}_{1_D} = \begin{pmatrix} 1 & & & \\ & -1 & & O \\ & & \ddots & \\ O & & & \end{pmatrix}_{D \times D} \tag{4}$$

and

$$\mathcal{C}_{2_D} = \begin{pmatrix} & & & 1 \\ O & & -1 & \\ & .\cdot^{\cdot} & & \\ & O & & \end{pmatrix}_{D \times D}. \tag{5}$$

The number of sublattices in each chain can be either odd or even, so there exist two types of formula for each symmetry. For the even number of sublattices per chain, the particle-hole and chiral symmetries satisfy the general relations $\mathcal{P}_i h(k) \mathcal{P}_i = -h^\star(-k)$ and $\Gamma_i h(k) \Gamma_i = -h(k)$ with $i = 1, 2$, respectively. When the R gets odd numbers, there are hidden particle-hole and chiral symmetries fulfilling $\mathcal{P}_i h(k) \mathcal{P}_i = -h^\star(-k - \pi)$ and $\Gamma_i h(k) \Gamma_i = -h(k - \pi)$, respectively. Note that all the operators of each symmetry can be commuted with each other as $[\mathbf{\Sigma}_i, \mathbf{\Sigma}_j] = 0$, where $\mathbf{\Sigma} = (\mathcal{T}, \mathcal{P}, \Gamma)$.

Due to $\mathcal{T}_i^2 = \mathcal{P}_i^2 = \Gamma_i^2 = I_{LR}$, according to the primary topological periodic table [10–13], which is based on nonspatial symmetries, the topological class of the system falls into BDI class with $\mathbb{Z}$ index and the band structure of the system may be gapped near the Fermi level revealing degenerate edge states in topologically nontrivial phases.

Furthermore, Hamiltonian Eq. (2) illustrates reflection and inversion symmetry. Although in quasi-1D systems, both inversion and reflection symmetries change $k \to -k$, they could have a different form of operators. The reflection and inversion symmetry defining $\Pi_i h(k) \Pi_i = h(-k)$ have the operators $\Pi_1 = I_L \otimes \tau_{x_R}$ and $\Pi_2 = \tau_{x_L} \otimes \tau_{x_R}$, respectively. Note that the inversion symmetry can be regarded as the reflection symmetry for each chain. The mirror line of reflection symmetry is perpendicular to the orientation of chains and bisects the system while the inversion symmetry has an inversion point located in the center of the system.

In addition to the main inversion symmetry, already discussed above, there is a subsidiary inversion symmetry whose inversion points can be placed between every two adjacent chains at the mirror line. This means that, under such symmetry, the system can be remained invariant by inverting every

two adjacent chains to each other with respect to the inversion point located between them. The operator of subsidiary inversion symmetry can be found as

$$\Pi_3 = \mathcal{C}_{3_L} \otimes \tau_{x_R}, \tag{6}$$

where

$$\mathcal{C}_{3_L} = \begin{pmatrix} 0 & 1 & & O \\ 1 & \ddots & \ddots & \\ & \ddots & \ddots & 1 \\ O & & 1 & 0 \end{pmatrix}_{L \times L}. \tag{7}$$

The first part of the Π_3 operator, i.e., $\mathcal{C}_{3_L}$ acts on the chain space and exchanges every two adjacent legs with each other, while the second part acts on the sublattice space of each leg and $x \to -x$. It should be noted that the subsidiary operator can satisfy inversion relation provided that the Π_1 is preserved.

B. Additional symmetries

In this system, as already mentioned, both the inversion and reflection symmetries can change k to $-k$, therefore, under a transformation that is a combination of the inversion with respect to the main inversion point and reflection with respect to the vertical mirror line, the Hamiltonian is invariant. This implies that there is an additional symmetry, namely, exchange symmetry, with a horizontal mirror line, along the x axis, in the middle of the lattice. Correspondingly, its exchange operator can be obtained by multiplying the reflection operator Π_1 by the inversion operator Π_2, i.e.,

$$\Upsilon_1 = \Pi_1 \Pi_2 = \tau_{x_L} \otimes I_R, \tag{8}$$

exchanging a chain from the upper half with its corresponding one in the lower half of the system. Also, the existence of the subsidiary inversion symmetry enables us to define a subsidiary exchange symmetry. Its operator is the matrix multiplication of Π_2 and Π_3,

$$\Upsilon_2 = \Pi_3 \Pi_2 = \mathcal{C}_{3_L} \otimes I_R, \tag{9}$$

exchanging two adjacent chains with respect to an axis, being parallel to the chains, located in the middle between them. Note, there would be Υ_2 as long as Υ_1 is established.

After obtaining the symmetries that leave the Hamiltonian invariant, it is possible to utilize them in dividing the system into subsystems by block diagonalizing the system Hamiltonian [61,62]. This makes it easy to inspect topological origins of system ingredients, in particular, when a system hosts finite-energy topological edge states [35]. Therefore, because of $[h(k), \Upsilon_i] = 0$ $(i = 1, 2)$, Hamiltonian Eq. (2) can be brought into a block-diagonal form through a unitary transformation $\mathcal{H}(k) = U h(k) U^{-1}$. The unitary matrix U can be constructed from the eigenstates of Υ_i. According to Eq. (8), it is easy to show that the eigenvalues of Υ_1 are ± 1. So, in the basis of Υ_1, the Hamiltonian will be block diagonalized into two decoupled blocks. If L is an even number, the size of both blocks is $LR/2$, while for odd L, the sizes of two blocks are $\lfloor \frac{L}{2} \rfloor R$ and $(1 + \lfloor \frac{L}{2} \rfloor)R$. In this case, one should find another exchange symmetry for each block and repeat the block-diagonalization process to obtain L blocks of size R.

On the other hand, the subsidiary exchange symmetry operator Υ_2 has L eigenvalues, λ_l, with R-fold degeneracy. The simple closed-form for the eigenvalues λ_l is [63,64]

$$\lambda_l = 2 \cos \left(\frac{l\pi}{L+1} \right), \quad l = 1, 2, ..., L. \tag{10}$$

So, in the Υ_2 representation, the Hilbert space of the system can be decomposed into L subspaces giving rise the Hamiltonian as $\mathcal{H}(k) = \bigoplus_{l=1}^{L} h_{\Upsilon_2 = \lambda_l}(k)$, where the Hamiltonian of each subsystem is

$$h_{\Upsilon_2 = \lambda_l}(k) = \begin{pmatrix} t\lambda_l & t & \dots & t'e^{-ik} \\ t & t\lambda_l & \ddots & \vdots \\ \vdots & \ddots & \ddots & t \\ t'e^{ik} & \dots & t & t\lambda_l \end{pmatrix}_{R \times R}. \tag{11}$$

Note that the Hamiltonian of subsystem Eq. (11) is a Hamiltonian of the extended SSH model [34,42,44,45], i.e., SSH$_R$, including R sublattices, with diagonal entries. Evidently, the multiplication of the coupling term t and the subsidiary exchange operator eigenvalues λ_l creates *effective on-site potentials* (see Eq. (11)). In analog to the original SSH chain model with $R = 2$, where there is only one gap, being the main gap, containing one pair of topological edge states in the topological regime, the subsystem SSH$_R$ has $R - 1$ gaps, including a main gap and subgaps. Each gap would host topological edge states. Consequently, in the present system with L subsystems, there could be a total of $L(R - 1)$ topological edge states with zero and/or finite energies.

It is worthwhile noting that if the L takes an even number, the system Hamiltonian is similar to an $L/2$-spinfull 1D system with SSH$_R$ chain that is exposed to an external Zeeman field with amplitude $t\lambda_l$. In this case, the exchange symmetry is equivalent to the spin-rotation symmetry in a 1D spinfull system [30]. For odd L, the system resembles an L-chain bosonic system with an integer spin $S = \lfloor L/2 \rfloor - 1$ [52].

As mentioned above, the topological phase transition occurs at $k = 0, \pi$ and $\theta/\pi = 1/2, 3/2$. By substituting these requirements in Eq. (11), the energy bands at the phase transition points can be obtained as [64]

$$E_{lr} = t \left[\lambda_l + 2 \cos \left(\frac{2r\pi - \pi}{R} \right) \right],$$
$$r = 1, 2, ..., R, \text{ if } k = \pi,$$
$$E_{lr} = t \left[\lambda_l + 2 \cos \left(\frac{2r\pi}{R} \right) \right],$$
$$r = 1, 2, ..., R, \text{ if } k = 0. \tag{12}$$

Subsequently, using Eqs. (10) and (12), gap closure conditions, i.e., $E_{lr} = 0$, implies that

$$k = 0 \to 2r = \frac{\pm Rl}{1 + L} + R, \tag{13}$$

$$k = \pi \to 2r - 1 = \frac{\pm Rl}{1 + L} + R. \tag{14}$$

Note, for $k = 0$ (π) the left-hand side of the above relation is a positive even (odd) quantity, since the r takes positive integer values. Also, for given integers R and L, the values of l satisfying in Eqs. (13) and (14) gives us the subsystems

that their gap can be closed and reopened at zero energy, namely, the main gap of the whole band structure. It is easy to show (see Appendix) that for such subsystems with the corresponding λ_l, the index l fulfills the following relation:

$$\frac{L+1}{m} \leqslant l \leqslant (m-1)\frac{L+1}{m}, \qquad (15)$$

where m is the greatest common divisor of $(L+1, R)$. From Eq. (15), one finds that there are $m-1$ subsystems for which main gap closing/reopening can take place. After the topological phase transition, the gap of each of these subsystems can contain one pair of zero-energy edge states. As a consequence, in total, there will be $m-1$ topological edge states at zero energy under open boundary conditions.

IV. SYMMETRIES OF THE SUBSYSTEMS

In this section, we will examine the symmetries of subsystems, i.e., Eq. (11). The subsystems have inversion and time-reversal symmetries. The corresponding operator of inversion symmetry is $\Pi' = \tau_{x_R}$ and of time-reversal symmetry is $\mathcal{T}' = I_R \mathcal{K}$. Depending on the value of λ_l, Eq. (11) can have extra symmetries as will be discussed in the following.

A. Odd numbers of L

In this case, the axis symmetry of the main exchange symmetry, Υ_1, coincides with the central chain and, at the same time, the number of eigenvalues of Υ_2, i.e., λ_l, will be an odd number. As a result, one of the eigenvalues λ_l must be zero originating from the fact that eigenvalues of a Hermitian operator, e.g., Υ_2, are symmetric about zero. This means that one of the subsystems whose effective on-site potential is zero, $t\lambda_l = 0$, has chiral symmetry. Such subsystem reminisces of the bare SSH_R system. However, the whole Hamiltonian has chiral symmetry. Depending on R that would take even or odd numbers, the system hosts topological edge states within either gapped or gapless bulk states around zero energy. Note that the subsystem corresponding to the zero eigenvalue has chiral and electron-hole symmetries in addition to the inversion and time reversal symmetry. The unitary part of particle-hole symmetry and chiral symmetry is $\mathcal{P}' = \Gamma' = \mathcal{C}_{1_R}$.

In fact, the even number of sublattices provides bulk insulating ground states supporting particle-hole and chiral symmetries in 1D systems [36–38,43–45]. Also, a pair of edge states manifests itself at zero energy because of the presence of inversion and chiral symmetry of the bare SSH_R subsystem [44,45]. So, the system at least hosts a pair of zero-energy edge states in a topological insulating regime. In the present cases, the chiral operators commute with the subsidiary exchange operator Υ_2 when the L takes odd numbers, i.e., $[\Gamma_i, \Upsilon_2] = 0$. As a consequence, according to Refs. [10–12], the class of the subsystem with $\lambda_l = 0$ (the subsystem with zero energy edge states) remains BDI, hosting nontrivial topological phases.

While the other subsystems lack chiral symmetry due to $\lambda_l \neq 0$ as already discussed above, these subsystems would have zero-energy edge states if Eqs. (13)–(15) established. In such a situation, $m > 1$ and the effective on-site potential forces the energy of finite-energy edge states of the corre-

sponding subsystems to be shifted toward zero energy. This is in contrast to the usual cases where there is no zero-energy topological edge state when there is no chiral symmetry [34]. Also, the topological classification of the subsystems without chiral symmetry belongs to AI class, owing to the presence of inversion and time-reversal symmetries in the subsystems [14–16].

On the other hand, an odd number of R providing an odd number of bands in each subsystem results in bulk metallic ground states, due to the existence of chiral symmetry and the subsystem with $\lambda_l = 0$ resides always within the gapless bulk states. Moreover, if conditions (13)–(15) are established in the other subsystems $\lambda_l \neq 0$, their zero-energy topological edge states would lie in the continuum instead of band gaps.

B. Even numbers of L

For an even number of chains, none of the eigenvalues of subsidiary exchange symmetry is zero. So, all the subsystems lack chiral symmetry though each chain may include either even or odd number sublattices. This implies that, unlike the previous case, there is not even one subsystem belonging to the BDI class. For an even or odd number of R, all subsystems have an AI class because of the inversion and time-reversal symmetries in the subsystems [14–16]. Moreover, the subsystems can be considered as the generalized SSH_R and have finite-energy edge states unless Eqs. (13)–(15) would be held for some of them.

C. Topological invariant

The existence of inversion symmetry in the subsystems gives rise that their Hamiltonians commute with the inversion symmetry operator at $k = 0$ and $k = \pi$. As such, the subsystems have well-defined parities. Also, the expectation value of inversion operator is ± 1 at either $k = 0$ or $k = \pi$. We can define topological invariant $\mathcal{N} = \sum_{l,r}^{L,R-1} |n_{0,l,r} - n_{\pi,l,r}|$ in $\mathbb{Z}$ [65], where $n_{0,l,r}$ and $n_{\pi,l,r}$ are the number of negative parities at $k = 0$ and $k = \pi$, respectively, for the lth subsystem and rth gap.

Actually, to distinguish localized and extended features of an eigenstate ψ_E in the corresponding eigenenergy E under open boundary conditions, we determine inverse participation ratio [66] as

$$I_E = \frac{Ln \sum_j |\psi_E(j)|^4}{Ln LRN}. \qquad (16)$$

In the above relation, the system would host localized and extended states, respectively, for $I_E = 0$ and $I_E = -1$.

V. PHASE DIAGRAM AND BAND STRUCTURES

In Fig. 3, we have plotted the phase diagram of system as function of R and L. The total numbers of topological edge states, $\mathcal{N}$, at both zero and finite energies, are represented by colors. According to Eq. (15), we specified the number of zero-energy edge states in the main gap by different colorful markers. For an odd number of R and L, there is a situation in which topological edge states in the gap of a subsystem can reside within the bulk states of another subsystem and the system can host topological edge states in the continuum. We
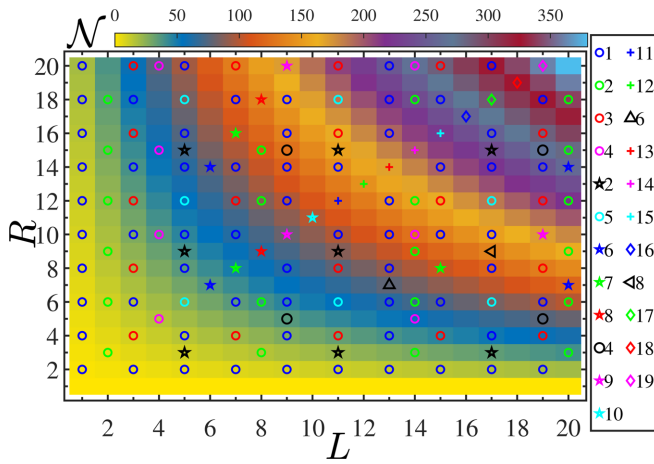
FIG. 3. Topological phase diagram of the system as functions of the chain number L and sublattice number R. The color indicates the total numbers of edge states ($\mathcal{N}$). Also, the colored and black markers represent the number of edge state in the main gap and in the continuum at zero energy, respectively. Note that the values of $\mathcal{N}$ are completely integers.

distinguish the number of edge states at zero energy in the continuum by black markers. One can see that $\mathcal{N}$ increases rapidly when both R and L increase rather that one of the parameters gets fixed values. Also, for a given L there are at most L zero-energy edge states in the main gap, if $R = p(L+1)$ where $p = 1, 2, 3, \ldots$.

The band structure and the related topological invariant $\mathcal{N}$ as a function of θ with $L = 2$ are shown in Figs. 4(a) and 4(c), respectively, for $R = 3$ and $R = 4$. In these cases, our system reduces to a two-leg ladder with three and four sublattices per leg. Because, here, the main exchange symmetry axis does not coincide on any chain, there is no zero eigenvalue for the subsidiary exchange symmetry operator Υ_2. Also, the whole system can be considered as a direct sum of two decoupled subsystems (or chains) with effective on-site potentials.

One can see in Fig. 4(a) that there are $L(R-1) = 4$ topological edge states in the topological regime with $\mathcal{N} = 4$. Also, according to $(L+1) = 3$ and $R = 3$, the great common divisor is $m = 3$, and therefore there exist $m - 1 = 2$ pairs of

zero-energy edge states in the main gap which are protected by inversion symmetry of their subsystem Hamiltonians. In this case, the effective on-site potential, originated from the combination of coupling term and eigenvalue of Υ_2, leads to shifting the finite-energy edge states to zero energy. Furthermore, the remaining $L(R-1) - (m-1) = 2$ topological edge states are finite-energy edge states within subgaps. Interestingly, for certain values of θ the finite-energy edges states cross the bulk states. In Fig. 4(b), the energy spectrum of the system versus wave function index corresponding to Fig. 4(a) is presented for $\theta/\pi = 1$. One can see that there are two (two) pairs of red stars at zero (finite) energy showing the number of nontrivial midgap zero- (finite-) energy edge states.

For the parameters of Fig. 4(c), we have $(L+1) = 3$ and $R = 4$ thus $m = 1$. As a result, the change of sublattice numbers causes the main gap to be closed. Subsequently, there is no zero-energy edge state, $m - 1 = 0$, and the total number of emerged edge states, $L(R-1) = 6$, would be hosted as finite-energy topological ones with $\mathcal{N} = 6$ in the topological regime. Correspondingly, as can be seen from Fig. 4(d), there are only six pairs of edge states, represented by red stars, distributed at different finite energies.

The band structures (with topological invariant $\mathcal{N}$) as a function of θ/π and wave-function index, respectively, in Figs. 5(a) and 5(b) are shown with $L = 5$ and $R = 3$. There are $L(R-1) = 10$ pairs of edge states in this case. L is odd, so one of the subsystems corresponding to $\lambda_l = 0$ has chiral symmetry. In addition, the odd number of R imposes that there is a band around zero energy. Also, there are $m - 1 = 2$ pairs of edge states at zero energy. These result in the presence of zero-energy edge states in the continuum, see Fig. 5(a). As shown in Fig. 5(b), there are six pairs of edge states at finite energy in the continuum, represented by blue stars. Also, we have shown extended bulk states (two pairs edge states in the gap) by white (red) stars.

VI. SYMMETRY BREAKING PERTURBATIONS

To demonstrate the effect of subsidiary exchange symmetry on topological features of the system, we invoke a perturbation to break this symmetry. Without loss of generality, we investigate a special case, for an odd number
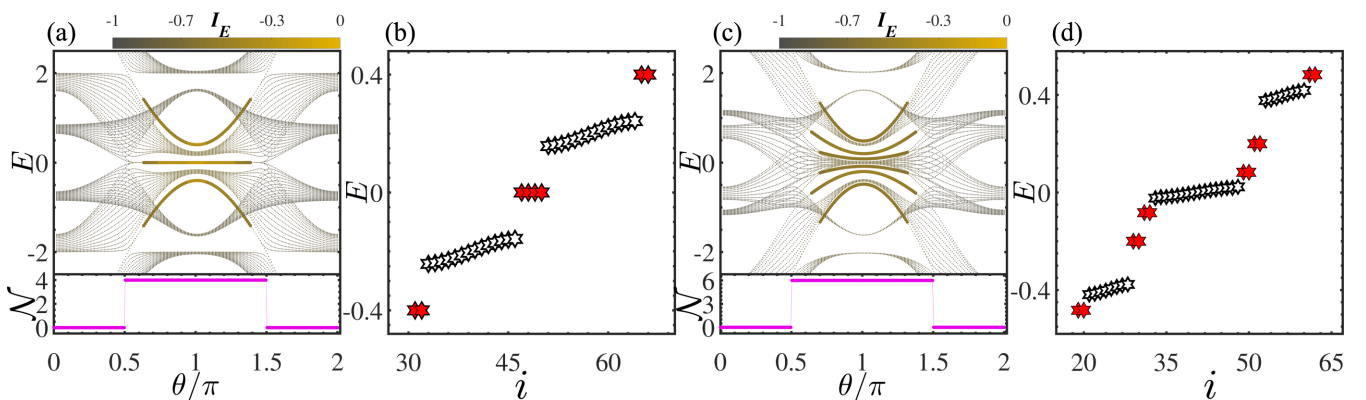
FIG. 4. Energy spectra and relevant topological invariant $\mathcal{N}$ as a function of θ/π under open boundary conditions for $L = 2$ with (a) $R = 3$ and (c) $R = 4$. The edge states appear in yellow and the extended bulk ones in gray color. (b), (d) Energy spectrum as a function of wave function index for the parameters used in (a) and (c), respectively, with $\theta/\pi = 1$. Edge and bulk states are shown by red and white stars, respectively.
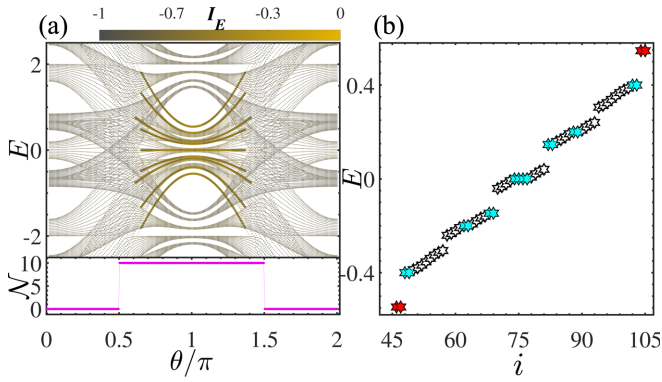
FIG. 5. (a) Energy spectra and relevant topological invariant as a function of θ/π under open boundary conditions with $(L, R) = (5, 3)$. The edge states are shown in yellow and the extended ones in gray color. (b) Energy spectrum as a function of wave function index corresponding to (a) with $\theta/\pi = 1$. The red, blue, and white markers represent, respectively, the edge states in the gap, the edge states in the continuum, and the extended bulk states.

of chains with even number of sublattices, $(L, R) = (3, 2)$. The subsidiary exchange symmetry, having Υ_2 operator, can be broken by setting either the intra- or intercell hopping amplitude of central chain different from the others, i.e., $t_{l=2} \neq t$ or $t'_{l=2} \neq t'$. Nevertheless, the system still has the main exchange symmetry with the Υ_1 operator. After diagonalization, the system can be considered as two decoupled blocks, i.e., SSH$_R$ and SSH$_{2R}$. So, there is no coupling term between the two subsystems and, interestingly, as shown in Fig. 6(a), the edge states of one block can lie within the bulk states of the other ones; the finite-energy edge states within $0.4 \lesssim \theta/\pi \lesssim 0.7$ and $1.3 \lesssim \theta/\pi \lesssim 1.6$. The breaking of the subsidiary exchange symmetry provides an off-diagonal term in one of the subsystems so the edge states of that block can be hybridized with its bulk states resulting in the finite-energy delocalized topological edge states in the continuum; the finite-energy edge states within $0.7 \lesssim \theta/\pi \lesssim 0.75$
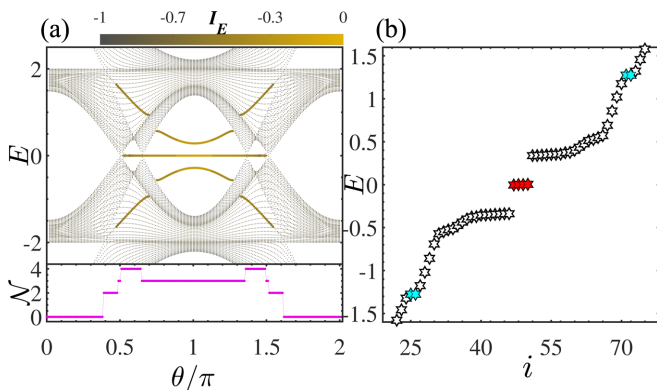
FIG. 6. (a) Dependence of energy spectra and relevant topological invariant on θ for $(L, R) = (3, 2)$. Here the parameters are the same as before except that $t_{l=2} = 0.1t$. (b) Energy spectrum as a function of wave function index corresponding to (a) with $\theta/\pi = 0.6$. Red, blue, and white markers represent, respectively, the edge states in the gap, the edge states in the continuum, and the extended bulk states.
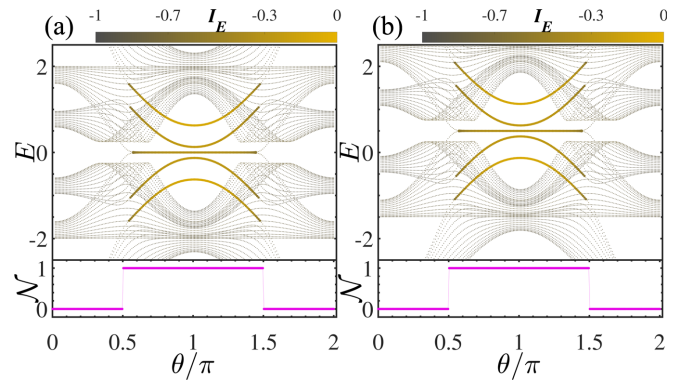
FIG. 7. Energy spectra and relevant topological invariant as a function of θ for $(L, R) = (3, 2)$. (a) $V_1 = 0.5, V_2 = 0$ (b) $V_1 = V_2 = 0.5$. By breaking the inversion symmetry of some subsystems and the whole system, the degeneracy of finite-energy edge states are destroyed and the gap around zero energy is opened.

and $1.25 \lesssim \theta/\pi \lesssim 1.3$. Although, one may expect that the system has $L(R - 1) = 3$ edge states (including one pair at zero energy), another gap around zero energy is opened and an extra one pair of edge states manifests itself in this gap. Thus, in total, the system hosts two pairs of edge states at zero energy and at finite energy, giving rise to four pairs of edge states within $0.5 \lesssim \theta/\pi \lesssim 0.6$ and $1.4 \lesssim \theta/\pi \lesssim 1.5$, see also Fig. 6(b).

Finally, let us ensure whether the inversion symmetry of subsystem is the fundamental symmetry protecting the edge states. To be more specific, we add the following perturbations:

$$H' = \sum_{n=1}^{N} \sum_{l=1}^{3} \sum_{r=1}^{2} [(-1)^r V_1 \delta_{l,2} + V_2] C_{n,l,r}^{\dagger} C_{n,l,r}, \quad (17)$$

to Hamiltonian Eq. (1) with parameters $(L, R) = (3, 2)$. Here, the $\delta_{l,l'}$ is the Kronecker delta and V_1 (V_2) is the amplitude of staggered (uniform) on-site potential breaking the inversion (chiral) symmetry of the full Hamiltonian. Despite breaking the subsidiary exchange symmetry, by rewriting the Hamiltonian in the basis of Υ_2, one subsystem corresponding to $\lambda_l = 0$ out of the three subsystems has inversion symmetry with operator

$$\Pi'_{\lambda_l=0} = \tau_{x_2}. \quad (18)$$

This subsystem inversion symmetry operator, clearly, acts on dimensions lower than those of the whole system. While the other two subsystems lack the inversion symmetry.

As shown in Fig. 7(a), for $V_1 \neq 0$ and $V_2 = 0$, one can see that the zero-energy edge state is preserved due to presence of the inversion symmetry for one of the subsystems, whereas the topology and the degeneracy of finite-energy edge states, related to the other two subsystems with broken inversion symmetry, are destroyed. Furthermore, turning on the V_2, breaking the full chiral symmetry, does not any effect on the subsystem-symmetry-protected edge states, as shown in Fig. 7(b). Consequently, importantly, the topology of the system is protected by the inversion symmetry of subsystems.

VII. SUMMARY

We considered the quasi-1D lattice system with L legs and R sublattices per leg. We determined symmetries of the system. It is shown that due to reflection and subsidiary inversion symmetry, the subsidiary exchange symmetry can be defined. Using this symmetry, we decomposed the system into subsystems. It is found the different topological phases can emerge, depending on L and R. In the topological regime, each subsystem reveals $R - 1$ topological edge states at zero and finite energy in the band structure. Consequently, there are, in total, $L(R - 1)$ topological edge states. For the case with nonzero eigenvalues of the subsidiary exchange symmetry, the corresponding subsystems lack chiral symmetry and these subsystems belong to the AI class. But when the axis of main exchange symmetry coincides on the central chain, due to vanishing one of the eigenvalues of subsidiary exchange symmetry, one of the subsystems would reduce to the original SSH$_R$ with chiral symmetry and this subsystem belongs to BDI class. The existence of topological edge states does not depend on the symmetry of the whole Hamiltonian. Instead, the inversion symmetry of the subsystems plays the key role in protecting the topological phases. Experimentally, the edges states can be observed in photonic lattices made of waveguide arrays [67].

APPENDIX: ALLOWED VALUES OF l AND THEIR NUMBER

In this Appendix, we determine which subsystems l host the topological edge states at zero energy. In other words, the possible values for l that can satisfy in Eq. (15) of the main text. Subsequently, we obtain the number of permissible value of l for given R and L.

Since Eqs. (13) and (14) of the main text contain positive integers R, $2r$, $2r - 1$, and L, so the expression $\frac{Rl}{L+1}$ should be an integer. The maximum value of l is L, so it is not possible to simplify this fraction unless there exists a greatest common divisor (GCD) between the two values $(L + 1, R)$. By introducing the GCD$(L + 1, R)$ as m, the fraction can be rewritten as $\frac{R}{m}\frac{ml}{L+1}$. Because $\frac{R}{m}$ is a positive integer, l should take the integer values $p\frac{L+1}{m}$ (with $p = 1, 2, 3, ...$) to enforce the fraction $\frac{R}{m}\frac{ml}{L+1}$ to be a positive integer.

Also $1 \leqslant l \leqslant L$, so

$$\frac{m}{L+1} \leqslant p \leqslant \frac{mL}{L+1}, \tag{A1}$$

where the lower bound is not integer and should be readjusted to 1 according to the lower value of p. The integer upper bound of p can be obtained as

$$\frac{mL}{L+1} = m - \frac{m}{L+1} < m, \tag{A2}$$

subsequently,

$$m - 1 \leqslant \frac{mL}{L+1} = m - \frac{m}{L+1}, \tag{A3}$$

resulting in

$$1 \leqslant p \leqslant m - 1. \tag{A4}$$

So, the allowed values of l are

$$\frac{L+1}{m} \leqslant l \leqslant (m-1)\frac{L+1}{m} \tag{A5}$$

and their number is $m - 1$.

[1] M. Z. Hasan and C. L. Kane, Rev. Mod. Phys. **82**, 3045 (2010).

[2] X.-L. Qi and S.-C. Zhang, Rev. Mod. Phys. **83**, 1057 (2011).

[3] M. Sato and Y. Ando, Rep. Prog. Phys. **80**, 076501 (2017).

[4] A. Bansil, H. Lin, and T. Das, Rev. Mod. Phys. **88**, 021004 (2016).

[5] N. R. Cooper, J. Dalibard, and I. B. Spielman, Rev. Mod. Phys. **91**, 015005 (2019).

[6] D.-W. Zhang, Y.-Q. Zhu, Y. X. Zhao, H. Yan, and S.-L. Zhu, Adv. Phys. **67**, 253 (2018).

[7] T. Ozawa, H. M. Price, A. Amo, N. Goldman, M. Hafezi, L. Lu, M. C. Rechtsman, D. Schuster, J. Simon, O. Zilberberg, and I. Carusotto, Rev. Mod. Phys. **91**, 015006 (2019).

[8] D. J. Thouless, M. Kohmoto, M. P. Nightingale, and M. den Nijs, Phys. Rev. Lett. **49**, 405 (1982).

[9] X.-G. Wen, Rev. Mod. Phys. **89**, 041004 (2017).

[10] A. P. Schnyder, S. Ryu, A. Furusaki, and A. W. W. Ludwig, Phys. Rev. B **78**, 195125 (2008).

[11] A. P. Schnyder, S. Ryu, A. Furusaki, and A. W. W. Ludwig, AIP Conf. Proc. **1134**, 10 (2009).

[12] S. Ryu, A. P. Schnyder, A. Furusaki, and A. W. W. Ludwig, New J. Phys. **12**, 065010 (2010).

[13] X.-G. Wen, Phys. Rev. B **85**, 085103 (2012).

[14] C.-K. Chiu, H. Yao, and S. Ryu, Phys. Rev. B **88**, 075142 (2013).

[15] K. Shiozaki and M. Sato, Phys. Rev. B **90**, 165114 (2014).

[16] C.-K. Chiu, J. C. Y. Teo, A. P. Schnyder, and S. Ryu, Rev. Mod. Phys. **88**, 035005 (2016).

[17] C. L. Kane and E. J. Mele, Phys. Rev. Lett. **95**, 146802 (2005).

[18] B. A. Bernevig, T. L. Hughes, and S. C. Zhang, Science **314**, 1757 (2006).

[19] J. E. Moore, Nature (London) **464**, 194 (2010).

[20] M. Z. Hasan and J. E. Moore, Annu. Rev. Condens. Matter Phys. **2**, 55 (2011).

[21] F. D. M. Haldane, Phys. Rev. Lett. **61**, 2015 (1988).

[22] L. Fu and C. L. Kane, Phys. Rev. Lett. **100**, 096407 (2008).

[23] Y. Tanaka, M. Sato, and N. Nagaosa, J. Phys. Soc. Jpn. **81**, 011013 (2012).

[24] S. M. Frolov, M. J. Manfra, and J. D. Sau, Nat. Phys. **16**, 718 (2020).

[25] A. A. Burkov and L. Balents, Phys. Rev. Lett. **107**, 127205 (2011).

[26] A. Burkov, Nat. Mater. **15**, 1145 (2016).

[27] B. Yan and C. Felser, Annu. Rev. Condens. Matter Phys. **8**, 337 (2017).

[28] N. P. Armitage, E. J. Mele, and A. Vishwanath, Rev. Mod. Phys. **90**, 015001 (2018).

[29] X. Ying and A. Kamenev, Phys. Rev. Lett. **121**, 086810 (2018).

[30] M. Bahari and M. V. Hosseini, Phys. Rev. B **99**, 155128 (2019).

[31] L. K. Upreti, C. Evain, S. Randoux, P. Suret, A. Amo, and P. Delplace, arXiv:1907.09914.

[32] M. Jangjan and M. V. Hosseini, Sci. Rep. **10**, 14256 (2020).

[33] S. Li, Z.-M. Yu, Y. Yao, and S. A. Yang, Front. Phys. **15**, 43201 (2020).

[34] M. Jangjan and M. V. Hosseini, Sci. Rep. **11**, 12966 (2021).

[35] N. F. Q. Yuan and L. Fu, Proc. Natl. Acad. Sci. USA **118**, e2019063118 (2021).

[36] W. P. Su, J. R. Schrieffer, and A. J. Heeger, Phys. Rev. Lett. **42**, 1698 (1979).

[37] W. P. Su, J. R. Schrieffer, and A. J. Heeger, Phys. Rev. B **22**, 2099 (1980).

[38] J. K. Asbóth, L. Oroszlány, and A. Pályi, *A Short Course on Topological Insulators* (Springer International Publishing, Cham, 2016).

[39] L. Li, Z. Xu, and S. Chen, Phys. Rev. B **89**, 085111 (2014).

[40] Z. Yan and S. Wan, Europhys. Lett. **107**, 47007 (2014).

[41] M. Bahari and M. V. Hosseini, Phys. Rev. B **94**, 125119 (2016).

[42] V. M. Martinez Alvarez and M. D. Coutinho-Filho, Phys. Rev. A **99**, 013833 (2019).

[43] M. Maffei, A. Dauphin, F. Cardano, M. Lewenstein, and P. Massignan, New J. Phys. **20**, 013023 (2018).

[44] D. Xie, W. Gou, T. Xiao, B. Gadway, and B. Yan, npj Quantum Inf. **5**, 55 (2019).

[45] M. Bahari and M. V. Hosseini, Physica E **119**, 113973 (2020).

[46] L. Kou, Y. Ma, Z. Sun, T. Heine, and C. Chen, J. Phys. Chem. Lett. **8**, 1905 (2017).

[47] M. A. Springer, T.-J. Liu, A. Kuc, and T. Heine, Chem. Soc. Rev. **49**, 2007 (2020).

[48] F. Liu and K. Wakabayashi, Phys. Rev. Lett. **118**, 076803 (2017).

[49] T. Giamarchi, Chem. Rev. **104**, 5037 (2004).

[50] A. Maiellaro, F. Romeo, and R. Citro, Eur. Phys. J.: Spec. Top. **227**, 1397 (2018).

[51] S. Gholizadeh, M. Yahyavi, and B. Hetenyi, Europhys. Lett. **122**, 27001 (2018).

[52] J. Zurita, C. E. Creffield, and G. Platero, Adv. Quantum Technol. **3**, 1900105 (2019).

[53] Y. Kuno, Phys. Rev. B **101**, 184112 (2020).

[54] N. Sun and L. K. Lim, Phys. Rev. B **96**, 035139 (2017)

[55] C. Li, S. Lin, G. Zhang, and Z. Song, Phys. Rev. B **96**, 125418 (2017).

[56] S.-L. Zhang and Q. Zhou, Phys. Rev. A **95**, 061601(R) (2017).

[57] S. Cheon, T.-H. Kim, S.-H. Lee, and H. W. Yeom, Science **350**, 182 (2015).

[58] Z. Guo, J. Jiang, H. Jiang, J. Ren, and H. Chen, Phys. Rev. Res. **3**, 013122 (2021).

[59] C. Yoon, C.-C. Liu, H. Min, and F. Zhang, arXiv:2005.14710.

[60] J. Huang, S. Li, C. Yoon, J. S. Oh, H. Wu, X. Liu, N. Dhale, Y.-F. Zhou, Y. Guo, Y. Zhang, M. Hashimoto, D. Lu, J. Denlinger, X. Wang, C. N. Lau, R. J. Birgeneau, F. Zhang, B. Lv, and M. Yi, Phys. Rev. X **11**, 031042 (2021).

[61] Y.-X. Xiao, Z.-Q. Zhang, and C. Chan, Sci. Rep. **8**, 5160 (2018).

[62] Y.-X. Xiao, G. Ma, Z.-Q. Zhang, and C. T. Chan, Phys. Rev. Lett. **118**, 166803 (2017).

[63] D. Kulkarni, D. Schmidt, and S.-K. Tsui, Linear Algebra Appl. **297**, 63 (1999).

[64] S. Noschese, L. Pasquini, and L. Reichel, Numer. Linear Algebra Appl. **20**, 302 (2013).

[65] T. L. Hughes, E. Prodan, and B. A. Bernevig, Phys. Rev. B **83**, 245132 (2011).

[66] B. Kramer and A. MacKinnon, Rep. Prog. Phys. **56**, 1469 (1993).

[67] G. Cáceres-Aravena, B. Real, D. Guzmán-Silva, A. Amo, L. E. F. Foa Torres, and R. A. Vicencio, Phys. Rev. Res. **4**, 013185 (2022).